Available online at www.sciencedirect.com

ScienceDirect

Mendeleev Commun., 2023, **33**, 487–490

Mendeleev Communications

Synthesis, crystal structure, and thermal behavior of Pt-based heterometallics $[PtPy_4](FcCOO)_2$ and *trans*-$[PtPy_2(FcCOO)_2]$

Ilya A. Yakushev,*[a] Nadezhda K. Ogarkova,[a,b] Evgeny V. Khramov,[a,c] Nadezhda S. Smirnova,[a,d] Maria Yu. Nesterenko,[a] Natalia V. Cherkashina,[a] Alexander G. Medvedev,[a] Maria V. Panina,[a] Michael N. Vargaftik[a] and Anna S. Popova[a,b]

[a] *N. S. Kurnakov Institute of General and Inorganic Chemistry, Russian Academy of Sciences, 119991 Moscow, Russian Federation. E-mail: ilya.yakushev@igic.ras.ru*
[b] *Peoples' Friendship University of Russia (RUDN University), 117198 Moscow, Russian Federation*
[c] *National Research Center 'Kurchatov Institute', 123182 Moscow, Russian Federation*
[d] *N. D. Zelinsky Institute of Organic Chemistry, Russian Academy of Sciences, 119991 Moscow, Russian Federation*

DOI: 10.1016/j.mencom.2023.06.015

Novel square-planar Pt-based heterometallic complexes with ferrocenecarboxylic acid were prepared in two steps from (tetrapyridine)platinum diacetate $[PtPy_4](OAc)_2$. The crystal structure of $[PtPy_4](FcCOO)_2$ and $[PtPy_2(FcCOO)_2]$ was established by single crystal X-ray diffraction. Subsequent thermal transformation of a trinuclear compound $[PtPy_2(FcCOO)_2]$ to a bimetallic Pt–Fe phase was studied by XAFS techniques.

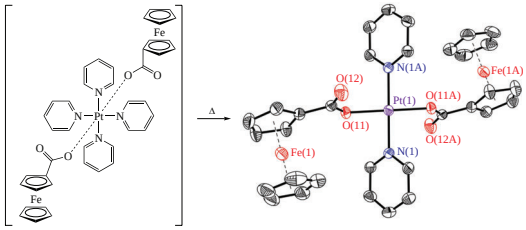

Keywords: platinum complexes, ferrocenecarboxylic acid, thermolysis, X-ray absorption spectroscopy, platinum–iron intermetallic compounds.

Study and modification of platinum metal coordination compounds, as well as of their chemical and physicochemical properties are of interest in connection with their potential value as homogeneous catalysts[1,2] and as precursors of supported catalysts[3,4] for various industrial chemical reactions and fine organic synthesis.[5] The transition from monometallic to heterometallic catalysts makes it possible to increase activity and reaction selectivity.[6,7] Importantly, the precursors of supported catalysts should not contain halides strongly bound to the metal center. In this regard, acetylacetonates[8] or carboxylic[9] compounds of the corresponding metals are frequently used; in particular, a carboxylate-based strategy is suitable to synthesize complexes with a non-equimolar metal-to-metal ratio.[10–14] One of the methods to introduce a heterometal into the compound is the use of metal-containing carboxylic acids (for example, ferrocenecarboxylic,[15] cymantrenecarboxylic,[16,17] *etc*.).

Previously, we have obtained catalytically active complexes of palladium with ferrocenecarboxylic acid, which can potentially be used as homogeneous catalysts[18] and precursors for supported catalysts.[19] The approach to Pt–Fe complexes differs from that of palladium-based complexes in the absence of a convenient synthetic protocol for producing mononuclear square-planar platinum-based complexes with carboxylic and N-donor ligands.

This work is devoted to the preparation of similar platinum complexes and the investigation of their possible application as precursors for supported bimetallic nanoparticles. The synthesis of such materials is determined by the fact that bimetallic Pt–Fe systems can be an effective catalyst in propane dehydrogenation,[20] oxygen reduction reaction[21] and selective hydrogenation in liquid phase.[22] The main advantage of using the heterobimetallic complex as a precursor is the obtaining of a homogeneous phase without admixtures of monometallic or oxide particles.

A suitable starting compound for the preparation of platinum ferrocene carboxylates is the previously described[23] complex $[PtPy_4](OAc)_2 \cdot 6H_2O$ **1**. Its reaction with ferrocenecarboxylic acid in methanol under mild conditions results in complex $[PtPy_4](FcCOO)_2 \cdot 2AcOH$ **2** (Scheme 1, step i) as the sole crystalline product (for the synthetic procedure, see Online Supplementary Materials). The next stage of the synthetic route (step ii) includes mild thermolysis under reduced pressure and leads to the trinuclear bimetallic complex *trans*-$[PtPy_2(FcCOO)_2]$ **3**. The sequential elimination of pyridine during thermolysis is also often observed for pyridine complexes of other transition metals, for example, oxalates of iron, cobalt, zinc, *etc*.[24] According to the TGA data (see Online Supplementary Materials, Figure S5), in contrast to the above complexes, the elimination of two pyridine molecules from $[PtPy_4](FcCOO)_2$ begins at essentially low temperatures (110–120 °C).

The structure of compound **2** may be presented as a cationic–anionic structure with the described earlier[25] $[PtPy_4]^{2+}$ cations and two ferrocenecarboxylate anions. Two solvating acetic acid molecules form hydrogen bonds with oxygen atoms related to the carboxylic group of the anion O(2S)–H···O(11) with an interatomic distance of 2.489(2) Å between the donor and the acceptor atom. The non-valent interaction of the oxygen atom of the anion with the central platinum atom Pt(1) is carried out directly through the ferrocenecarboxylate anion, and the Pt(1)–O(12) distance is 3.6355(15) Å.[†]

[†] *Crystal data for* **2**. $C_{46}H_{46}Fe_2N_4O_8Pt$, $M = 1089.66$, monoclinic, $a = 9.2623(4)$, $b = 8.7965(4)$ and $c = 26.4081(13)$ Å, $\alpha = 90$,

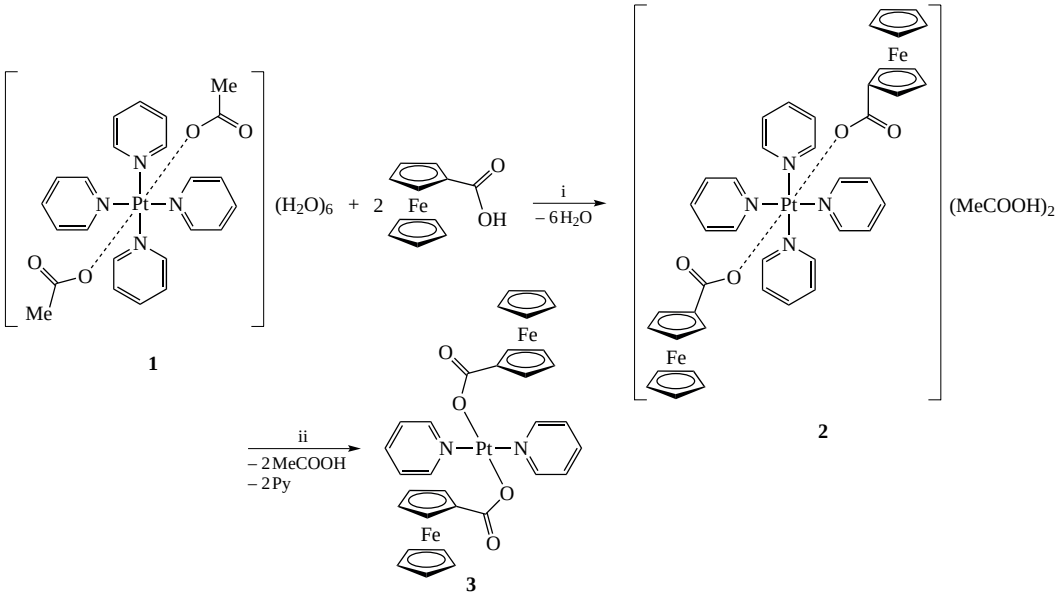

Scheme 1 *Reagents and conditions*: i, FcCOOH (2 equiv.), MeOH; ii, reduced pressure, 90 °C.

Compound *trans*-[$PtPy_2(FcCOO)_2$] **3** is the elimination product of two pyridine molecules from complex **2** followed by rearrangement of non-volatile ferrocenecarboxylic anions to the platinum atom Pt(1) straightforward *via* platinum to oxygen bond Pt–O formation. Complex **3** crystallizes‡ in the triclinic space group $P\bar{1}$ without additional solvent molecules, and by chemical composition and molecular structure similar to palladium-based ferrocenecarboxylates with monodentate pyridine-like ligands.[18,19] The central atom Pt(1) occupied the inversion center and was surrounded by two nitrogen atoms and two oxygen atoms in trans-position each with interatomic distances of 2.012(2) Å and 2.0145(19) Å for Pt(1)–N(1) and Pt(1)–O(11), respectively, which are common values for well-studied palladium complexes,[30] as well as general molecular geometry of the central platinum atom in less investigated platinum-based carboxylates.[31,32] As expected, interatomic distances between platinum atoms Pt(1) and iron atoms Fe(1) in **2** and **3** are different: Pt(1)–Fe(1) is 6.6613(4) Å for **2** and 5.4864(7) Å for **3**.

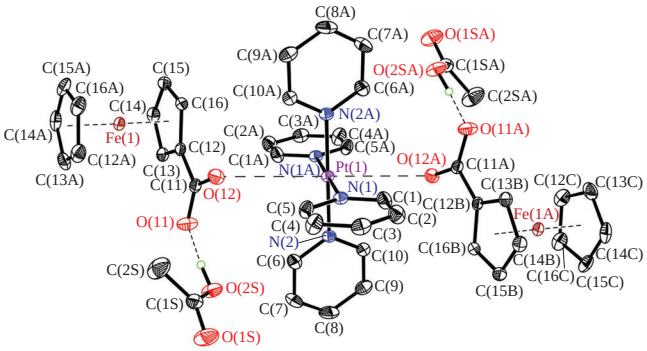

Figure 1 Molecular structure and numbering scheme for compound $[PtPy_4](FcCOO)_2 \cdot 2\,MeCOOH$ **2**. Atomic thermal displacement parameters are shown at a 50% probability level.

X-ray absorption spectroscopy (EXAFS and XANES) data for temperature transformations of the $PtPy_2(FcCOO)_2$ complex are shown in Figures S6 and S7 (see Online Supplementary Materials). The white line of Pt L_3 XANES spectra of the initial complex is larger than that of the Pt reference foil, indicating that platinum is presented in oxidized state [see Figure S6(*a*)]. An increase in temperature from 25 to 120–125 °C results in a gradual decrease in white line intensity and a broadening of XAFS oscillations. The heating to 400 °C in reducing atmosphere results in different shape and lower intensity of the white line, revealing the transition of platinum to the zerovalent state. As displayed in Figure 2, a platinum atom in the initial state of complex **3** is surrounded by two oxygen and two nitrogen atoms. The presence of an intensive peak at ~1.6–2.0 Å in the Fourier transformations of the EXAFS spectrum of the initial sample corresponds to Pt–O and Pt–N coordination spheres [see Figure S6(*b*)]. According to modeling results (Table S2), a growth of the coordination number from 2 to 4 for the Pt–O shell can be associated with distortion of the initial form of the complex or with the possible presence of solvent molecules. The distance between Pt and Fe is 5.4 Å, which is too far to be visible by the EXAFS method.

β = 97.0517(17) and γ = 90°, V = 2135.35(17) Å^3, space group $P2_1/c$, Z = 2, d_{calc} = 1.695 g cm^{-3}, $F(000)$ = 1088, $\mu(MoK_\alpha)$ = 3.997, yellow prism with dimensions *ca.* 0.45 × 0.23 × 0.20. A total of 41 464 reflections (6515 unique, R_{int} = 0.0390) were measured with a Bruker D8 Venture diffractometer (graphite monochromatized MoK_α radiation, λ = 0.71073 Å) using ω- and φ-scan modes at 100 K. The final residuals were R_1 = 0.0204 for 5523 reflections with $I > 2\sigma(I)$ and wR_2 = 0.0430 for all data and 282 parameters. GoF = 1.075.

‡ *Crystal data for* **3**. $C_{32}H_{28}Fe_2N_2O_4Pt$, M = 811.35, triclinic, a = 6.0077(6), b = 7.8469(8) and c = 15.6354(16) Å, α = 76.863(5), β = 81.194(5) and γ = 84.290(5)°, V = 707.73(13) Å^3, space group $P\bar{1}$, Z = 1, d_{calc} = 1.904 g cm^{-3}, $F(000)$ = 396, $\mu(MoK_\alpha)$ = 5.982, yellow prism with dimensions *ca.* 0.12 × 0.06 × 0.005. A total of 17 592 reflections (4299 unique, R_{int} = 0.0430) were measured with a Bruker D8 Venture diffractometer (graphite monochromatized MoK_α radiation, λ = 0.71073 Å) using ω- and φ-scan modes at 100 K. The final residuals were R_1 = 0.0257 for 4173 reflections with $I > 2\sigma(I)$ and wR_2 = 0.0568 for all data and 187 parameters. GoF = 1.038.

The data were corrected for absorption effects using the SADABS[26] software. The structures were solved by direct methods[27] and refined by full-matrix least squares technique[28] on F^2 with anisotropic displacement parameters for all non-hydrogen atoms. The hydrogen atoms were placed in calculated positions and refined using a riding model with fixed isotropic displacement parameters [U_{iso}(H) = 1.5 U_{eq}(C) for methyl groups and U_{iso}(H) = 1.2 U_{eq}(C) for all other H-atoms], except H-atoms of the carboxylic-group solvating acetic acid in **2**. The acidic hydrogen atom was located from the Fourie difference map and refined isotopically without additional restraints. All calculations were carried out using the SHELXTL[27] program and Olex2 X-ray data visualization program package.[29] For details, see Online Supplementary Materials, Table S1.

CCDC 2203709 and 2203710 contain the supplementary crystallographic data for this paper. These data can be obtained free of charge from The Cambridge Crystallographic Data Centre *via* http://www.ccdc.cam.ac.uk.

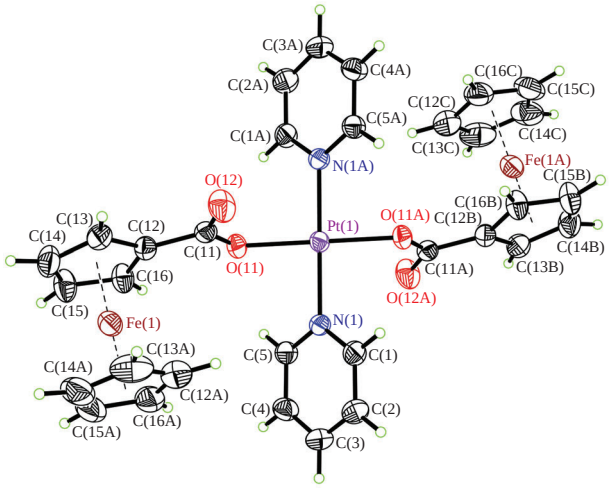

Figure 2 Crystal structure and numbering scheme for *trans*-[$PtPy_2(FcCOO)_2$] **3**. Atomic thermal displacement parameters are shown at a 35% probability level.

The heating of sample **3** from 25 to 100–110 °C in a H_2/He flow leads to a slight decrease in the intensity of the Pt–-O(N) peak [see Figure S6(*b*)]. Raising the temperature from 120 to 165 °C results in a decrease in the Pt–O(N) peak intensity with simultaneous appearance of a peak at ~2.5–2.8 Å corresponding to the first-shell Pt–Pt distance of metallic platinum. Further reduction of the sample with the temperature growth from 200 to 400 °C promotes the formation of the bimetallic Pt–Fe phase, which follows from a shift of the maximum of the Pt–Pt peak towards smaller interatomic distances. The shape of the XANES FeK spectrum for the initial sample corresponds to the oxidized state of iron at ambient conditions (see Figure S7). Heating of the complex to 125–145 °C in a H_2/He flow keeps the local environment of iron almost unchanged. Noticeable changes in the shape of the white line are observed when the temperature reaches ⩾200 °C. Further reduction at 400 °C does not lead to significant changes in the XANES spectra of the FeK-edge.

According to XRD data of the initial bimetallic complex, the iron atom is located between two ferrocene rings (ten carbon atoms at 2.02 Å), which is confirmed by EXAFS modeling (Table S2; CN of the Fe–C shell is 9.7, which is very close to 10). In contrast to the platinum edge, where the transformation occurs already at 120 °C, the iron environment remains stable up to 165 °C. When the temperature reaches 250 °C, the intensive peak of Fe–C disappears with the simultaneous formation of the Fe–M (where M = Pt or Fe) peak at ~2.5–2.7 Å, indicating the formation of the bimetallic phase. Further heating to 400 °C does not lead to principal changes in EXAFS and XANES spectra. These results are consistent with TGA/DSC data (Figure S5).

According to the phase diagram of the Pt–Fe system,[33,34] there are two intermetallic phases $PtFe_3$ and PtFe, which can be formed in the range from 20 to 60 at% of platinum. Results of modeling products after reduction at 400 °C and subsequent cooling to room temperature shows the formation of an equimolar tetragonal PtFe compound (Table S3 and Figure S8). Adding another shell of a metallic Fe or an iron-rich $PtFe_3$ compound to the model does not improve the R-factor.

To conclude, the current work demonstrates the possibility of producing heteronuclear cation–anion complexes of (tetrapyridine)platinum(II) with metal-containing ferrocenecarboxylic acid $[PtPy_4](FcCOO)_2 \cdot 2AcOH$. Its mild thermolysis leads to a trinuclear Pt–Fe complex *trans*-$[PtPy_2(FcCOO)_2]$. The subsequent thermal transformation of *trans*-$[PtPy_2(FcCOO)_2]$ in reductive atmosphere leads to the formation of a bimetallic PtFe phase.

This study was supported by the Russian Science Foundation (grant no. 18-73-10206-P). The research was performed using the equipment of the JRC PMR IGIC RAS.

Online Supplementary Materials

Supplementary data associated with this article can be found in the online version at doi: 10.1016/j.mencom.2023.06.015.

References

1 I. P. Stolarov, I. A. Yakushev, A. V. Churakov, N. V. Cherkashina, N. S. Smirnova, E. V. Khramov, Y. V. Zubavichus, V. N. Khrustalev, A. A. Markov, A. P. Klyagina, A. B. Kornev, V. M. Martynenko, A. E. Gekhman, M. N. Vargaftik and I. I. Moiseev, *Inorg. Chem.*, 2018, **57**, 11482.
2 Y. Hu and C. Wang, *Acta Phys.-Chim. Sin.*, 2019, **35**, 913.
3 S. Wang, D. Zhang, Y. Ma, H. Zhang, J. Gao, Y. Nie and X. Sun, *ACS Appl. Mater. Interfaces*, 2014, **6**, 12429.
4 G. Saravanan, K. P. Jayasree, Y. Divya, M. Pallavi and L. Nitin, *Intermetallics*, 2018, **94**, 179.
5 P. Buchwalter, J. Rosé and P. Braunstein, *Chem. Rev.*, 2015, **115**, 28.
6 N. Norouzi, M. K. Das, A. J. Richard, A. A. Ibrahim, H. M. El-Kaderi and M. S. El-Shall, *Nanoscale*, 2020, **12**, 19191.
7 Y. Shu, L. E. Murillo, J. P. Bosco, W. Huang, A. I. Frenkel and J. G. Chen, *Appl. Catal., A*, 2008, **339**, 169.
8 M. Radlik, A. Śrębowata, W. Juszczyk, K. Matus, A. Małolepszy and Z. Karpiński, *Adsorption*, 2019, **25**, 843.
9 J. Váňa, J. Bartáček, J. Hanusek, J. Roithová and M. Sedlák, *J. Org. Chem.*, 2019, **84**, 12746.
10 N. Yu. Kozitsyna, A. E. Gekhman, S. E. Nefedov, M. N. Vargaftik and I. I. Moiseev, *Inorg. Chem. Commun.*, 2007, **10**, 956.
11 S. E. Nefedov, I. A. Yakushev, N. Yu. Kozitsyna, Z. V. Dobrokhotova, V. N. Ikorsky, M. N. Vargaftik and I. I. Moiseev, *Inorg. Chem. Commun.*, 2007, **10**, 948.
12 M. A. Shmelev, Yu. K. Voronina, S. S. Chekurova, N. V. Gogoleva, T. M. Ivanova, O. I. Lyamina, E. V. Fatyushina, M. A. Kiskin, A. A. Sidorov and I. L. Eremenko, *Russ. J. Coord. Chem.*, 2021, **47**, 551 (*Koord. Khim.*, 2021, **47**, 489).
13 I. A. Yakushev, N. V. Cherkashina, N. S. Smirnova, M. N. Vargaftik, M. A. Dyuzheva and A. B. Kornev, *J. Struct. Chem.*, 2021, **62**, 1511 (*Zh. Strukt. Khim.*, 2021, **62**, 1616).
14 I. A. Yakushev, E. A. Sosunov, Yu. E. Makarevich, A. D. Maksimova, M. Yu. Nesterenko and M. N. Vargaftik, *J. Struct. Chem.*, 2022, **63**, 1997 (*Zh. Strukt. Khim.*, 2022, **63**, 103431).
15 S. Tanaka and K. Mashima, *Inorg. Chem.*, 2011, **50**, 11384.
16 S. S. Shapovalov, A. V. Gordienko, A. A. Pasynskii, Yu. V. Torubaev, I. V. Skabitskii and G. G. Aleksandrov, *Russ. J. Coord. Chem.*, 2011, **37**, 447 (*Koord. Khim.*, 2011, **37**, 445).
17 A. A. Pasynskii and S. S. Shapovalov, *Russ. J. Coord. Chem.*, 2016, **42**, 574 (*Koord. Khim.*, 2016, **42**, 532).
18 A. S. Popova, N. K. Ogarkova, S. S. Shapovalov, I. V. Skabitsky, E. K. Kultyshkina, I. A. Yakushev and M. N. Vargaftik, *Mendeleev Commun.*, 2022, **32**, 576.
19 I. A. Yakushev, M. A. Dyuzheva, I. A. Stebletsova, A. B. Kornev, N. V. Cherkashina and M. N. Vargaftik, *Russ. J. Coord. Chem.*, 2022, **48**, 153 (*Koord. Khim.*, 2022, **48**, 157).
20 E. C. Wegener, B. C. Bukowski, D. Yang, Z. Wu, A. J. Kropf, W. N. Delgass, J. Greeley, G. Zhang and J. T. Miller, *ChemCatChem*, 2020, **12**, 1325.
21 L. Cao, W. Liu, Q. Luo, R. Yin, B. Wang, J. Weissenrieder, M. Soldemo, H. Yan, Y. Lin, Z. Sun, C. Ma, W. Zhang, S. Chen, H. Wang, Q. Guan, T. Yao, S. Wei, J. Yang and J. Lu, *Nature*, 2019, **565**, 631.
22 A. A. Shesterkina, O. P. Tkachenko, E. V. Shuvalova, G. I. Kapustin, V. B. Kazansky and L. M. Kustov, *Mendeleev Commun.*, 2019, **29**, 666.
23 I. A. Yakushev, M. Yu. Nesterenko, P. V. Dorovatovskii, A. B. Kornev, A. D. Maksimova, A. S. Popova, N. V. Cherkashina, A. V. Churakov and M. N. Vargaftik, *Russ. J. Coord. Chem.*, 2022, **48**, 935 (*Koord. Khim.*, 2023, **49**, 51).
24 V. Jordanovska and S. Aleksovska, *Macedonian Academy of Sciences and Arts, Contributions, Section of Mathematical and Technical Sciences*, 1988, **9**, 65.
25 C. H. Wei, B. E. Hingerty and W. R. Busing, *Acta Crystallogr.*, 1989, **C45**, 26.
26 L. Krause, R. Herbst-Irmer, G. M. Sheldrick and D. Stalke, *J. Appl. Crystallogr.*, 2015, **48**, 3.
27 G. M. Sheldrick, *Acta Crystallogr.*, 2015, **A71**, 3.

28 G. M. Sheldrick, *Acta Crystallogr.*, 2015, **C71**, 3.
29 O. V. Dolomanov, L. J. Bourhis, R. J. Gildea, J. A. K. Howard and H. Puschmann, *J. Appl. Crystallogr.*, 2009, **42**, 339.
30 M. Gudenschwager and M. S. Wickleder, *Z. Kristallogr. – New Cryst. Struct*., 2013, **228**, 165.
31 C. R. Bondy, P. A. Gale and S. J. Loeb, *Supramol. Chem.*, 2002, **2**, 93.
32 N. V. Cherkashina, D. I. Kochubey, V. V. Kanazhevskiy, V. I. Zaikovskii, V. K. Ivanov, A. A. Markov, A. P. Klyagina, Z. V. Dobrokhotova, N. Yu. Kozitsyna, I. B. Baranovsky, O. G. Ellert, N. N. Efimov, S. E. Nefedov, V. M. Novotortsev, M. N. Vargaftik and I. I. Moiseev, *Inorg. Chem.*, 2014, **53**, 8397.
33 O. K. von Goldbeck, *IRON – Binary Phase Diagrams*, Springer, Berlin, Heidelberg, 1982.
34 Z. Wen, Y. Wang, C. Wang, M. Jiang, H. Li, Y. Ren and G. Qin, *Int. J. Mater. Res.*, 2022, **113**, 428.

Received: 21st December 2022; Com. 22/7072